DOI: 10.1002/chem.200903201

Interaction of Antifreeze Proteins with Hydrocarbon Hydrates

Hiroshi Ohno,[a, b] Robin Susilo,[a, b] Raimond Gordienko,[b] John Ripmeester,*[a] and Virginia K. Walker*[b]

Abstract: Recombinant antifreeze proteins (AFPs), representing a range of activities with respect to ice growth inhibition, were investigated for their abilities to control the crystal formation and growth of hydrocarbon hydrates. Three different AFPs were compared with two synthetic commercial inhibitors, poly-*N*-vinylpyrrolidone (PVP) and HIW85281, by using multiple approaches, which included gas uptake, differential scanning calorimetry (DSC) temperature ramping, and DSC isothermal observations. A new method to assess the induction period before heterogeneous nucleation and subsequent hydrate crystal growth was developed and involved the dispersal of water in the pore space of silica gel beads. Although hydrate nucleation is a complex phenomenon, we have shown that it can now be carefully quantified. The presence of AFPs delayed crystallization events and showed hydrate growth inhibition that was superior to that of one of the benchmark commercial inhibitors, PVP. Nucleation and growth inhibition were shown to be independent processes, which indicates a difference in the mechanisms required for these two inhibitory actions. In addition, there was no apparent correlation between the assayed activities of the three AFPs toward hexagonal ice and the cubic structure II (sII) hydrate, which suggests that there are distinctive differences in the protein interactions with the two crystal surfaces.

Keywords: adsorption · antifreeze proteins · clathrates · hydrates · inhibitors · proteins

Introduction

Clathrate hydrates (also called gas hydrates) are ice-like crystalline solids that form when hydrogen-bonded water cage structures enclathrate small molecules under appropriate conditions (pressure (*P*), time (*t*), and concentration).[1] For gaseous guests such as natural gas components, hydrates form at moderately low temperatures and high pressures.[1] Vast quantities of natural gas hydrate exist in offshore sediments on the continental margins[2] and under the permafrost in the Arctic.[3] Gas hydrate plugs can also block gas and oil pipelines, and on occasion, such plugs may have catastrophic economic and environmental consequences.[4] The structures and equilibrium thermodynamics of hydrates are reasonably well understood,[1,5] so for some time now attention has been focused on understanding hydrate processes in the expectation that this will lead to the ability to control both hydrate decomposition and formation. In the case of the former, controlled hydrate decomposition will help to realize the potential of producing gas from natural gas hydrates. In the case of the latter, the control of gas hydrate formation to avoid pipeline plugs during natural gas and oil production and transportation is a major concern of the energy industry.[6] Although hydrate plug formation is commonly prevented with thermodynamic inhibitors, such as methanol or glycol, which depress hydrate dissociation temperatures, this is costly due to the high concentrations of additives required (up to $\approx$50 wt% of the water phase) and these inhibitors can themselves cause environmental pollution. As a result of these drawbacks, there has been a movement to introduce new kinetic hydrate inhibitors (KHIs). These usually are water-soluble polymers that significantly delay hydrate nucleation and/or postnucleation crystal growth, even at low concentrations (less than 1 wt% of the water phase).[6,7] Although details of the KHI inhibition mechanisms are not understood, these molecules are

[a] Dr. H. Ohno, Dr. R. Susilo, Dr. J. Ripmeester
Steacie Institute for Molecular Sciences
National Research Council Canada
Ottawa, Ontario K1A 0R6 (Canada)
Fax: (+1) 613-998-7833
E-mail: John.Ripmeester@nrc.ca

[b] Dr. H. Ohno, Dr. R. Susilo, R. Gordienko, Dr. V. K. Walker
Department of Biology
Queen's University
Kingston, Ontario K7L 3N6 (Canada)
Fax: (+1) 613-533-6617
E-mail: walkervk@queensu.ca

thought to adsorb to growing hydrate crystal surfaces. The energy sector anticipates that deeper sea gas and oil fields will be exploited in the future, with the increasing probability of encountering conditions that are more favorable for hydrate formation, so the development of high-performance hydrate inhibitors is of major importance.[4,6]

Antifreeze proteins (AFPs) have evolved independently in different organisms to protect them from low-temperature freeze damage by adsorbing to ice and acting as kinetic inhibitors of crystal growth.[8] They are divergent structurally[9] but can be categorized according to their activities toward ice, because by adsorbing to the ice surface, they depress the freezing point but have little effect on the melting point. This temperature difference can be assayed and is known as thermal hysteresis (TH). AFPs with low TH are frequently found in freeze-tolerant plants, including perennial rye grass, *Lolium perenne* (Lp AFP),[10] whereas AFPs with moderate TH activities ($\approx$1 °C) are found in some freeze-intolerant fish that frequent ice-laden ocean waters, such as the ocean pout (type III AFP).[11] 'Hyperactive' AFPs with several degrees of TH have been found in certain insects, including the beetle *Tenebrio molitor* (Tm AFP).[12] Despite differences in the crystal structures of ice and gas hydrates, several AFPs have been shown to modify the crystal morphology of structure II (sII) tetrahydrofuran (THF) hydrate and ice, in addition to retarding hydrate nucleation better than a standard commercial KHI, poly-*N*-vinylpyrrolidone (PVP).[13–15] It should be noted that, although THF hydrate is not a 'gas' hydrate, it has been widely used as a convenient model system due to its mild formation conditions: it melts at approximately 4 °C at atmospheric pressure.[5] Nevertheless, caution needs to be exercised in assuming that the results for hydrates formed with highly water-soluble guests can be extrapolated to natural gas hydrates.[16] We have also shown that the nucleation and growth of both sII and structure I (sI) hydrates with propane and methane gases can be inhibited in the presence of a fish type I AFP.[17] Others have also noted the effect of AFPs on hydrate formation: Uchida et al. observed that type III AFP increased the induction period for crystallization and reduced the growth rate of sI CO_2–hydrate films,[18] and Al-Adel et al. reported that the influence of type I AFP on methane hydrate formation depends on the free-energy "driving force" (ΔG) available and that, at certain temperatures and pressures, the protein even appeared to act as a crystal growth promoter.[19]

Together, these reports have shown the potential of non-toxic AFPs as alternative hydrate inhibitors, and these proteins have thus attracted the attention of both academics and industrialists alike.[20] Most previous studies on the action of inhibitors on gas hydrates have put emphasis on growth inhibition after hydrate nucleation with just one or two induction-time measurements. However, the stochastic nature of nucleation phenomena requires statistical analysis. Reproducibly robust experiments on nucleation and subsequent growth events are essential for a comprehensive understanding of hydrate inhibition by AFPs. We also believe that it is important to use a natural gas composition for evaluation because the kinetics of hydrate formation is at least partially dictated by the guest molecules. Herein, we show the effects of several AFPs, representing all three categories of TH ice activity, as well as two commercial KHIs, on both the nucleation and growth of natural gas hydrates formed from a methane–ethane–propane gas mixture. Multiple characterization methods were employed in order to compare data obtained from divergent systems to investigate the relationship between inhibition and driving force, nucleation and growth inhibition, hydrate and ice inhibition, and the time dependence of nucleation inhibition. We also present a new method to study nucleation phenomena that is relatively free from mass-transfer limitations, uses small amounts of materials, and allows multiple experiments to be carried out in parallel.

Results and Discussion

Gas uptake: Induction times were determined as the time of the initial drop in gas pressure after the system reached equilibrium at 16.6 °C and 6.7 MPa (calculated with CSMGem;[21] not shown). Samples containing inhibitors or proteins showed longer induction times than control samples (Table 1), which suggested nucleation inhibition effects. The observed decrease in pressure associated with hydrate formation was converted into the hydrate gas consumption by using a gas equation of state with suitable compressibility factors calculated by Pitzer's correlations[22] (not shown). For these calculations, the gas composition was assumed to be constant (actually, the gas composition changes during the reaction due to preferential enclathration of larger gas molecules; this results in an experimental error of less than two percent) and dissolved gas in the liquid phase was ignored. The mean gas consumption was subsequently converted into water-to-hydrate conversion ratios by using the assumption of an average cage occupancy of 0.95 (CSMGem[21] sII); for all samples, the overall hydrate growth was reproducible for each repeated sample (not shown). Without inhibitors or

Table 1. Mean induction times of methane–ethane–propane hydrate nucleation observed in gas-uptake experiments for fresh, $t_{i,\,fresh}$, and recrystallized, $t_{i,\,repeat}$, samples with and without inhibitors.

Sample[a]	$t_{i,\,fresh}$ [s][b]	$t_{i,\,repeat}$ [s][b]
control	645	65
type III AFP	1955	95
type III AFP–GFP	2375	75
LpAFP–GFP	3960	75
TmAFP	1260	60
GFP	2680	100
PVP	1840	140
HIW85281	5060	95

[a] All inhibitors were used at a concentration of 0.1 mM. [b] The CSMGem[21] statistical program was used for the calculation of the incipient (i) hydrate phase equilibrium.

proteins, hydrate formation was complete in approximately 1000 min for fresh runs and about 1800 min for recrystallization runs (Figure 1). In contrast, samples containing additives had hydrate conversion rates that were significantly lower (Figure 1), and furthermore, even after extended times, they had not yet reached completion. Substantial inhibition of hydrate formation was seen with AFPs (Figure 1). The most effective inhibitors were type III AFP, TmAFP, and HIW85281. Type III AFP–GFP and LpAFP–GFP showed intermediate values, and even GFP performed better than the benchmark commercial inhibitor, PVP. For all samples, the water-to-hydrate conversion ratio was about 0.7–0.8 at the conclusion of the experiments, which suggests that the presence of inhibitor did not change the final amount of hydrate formed under the conditions of the experiments.

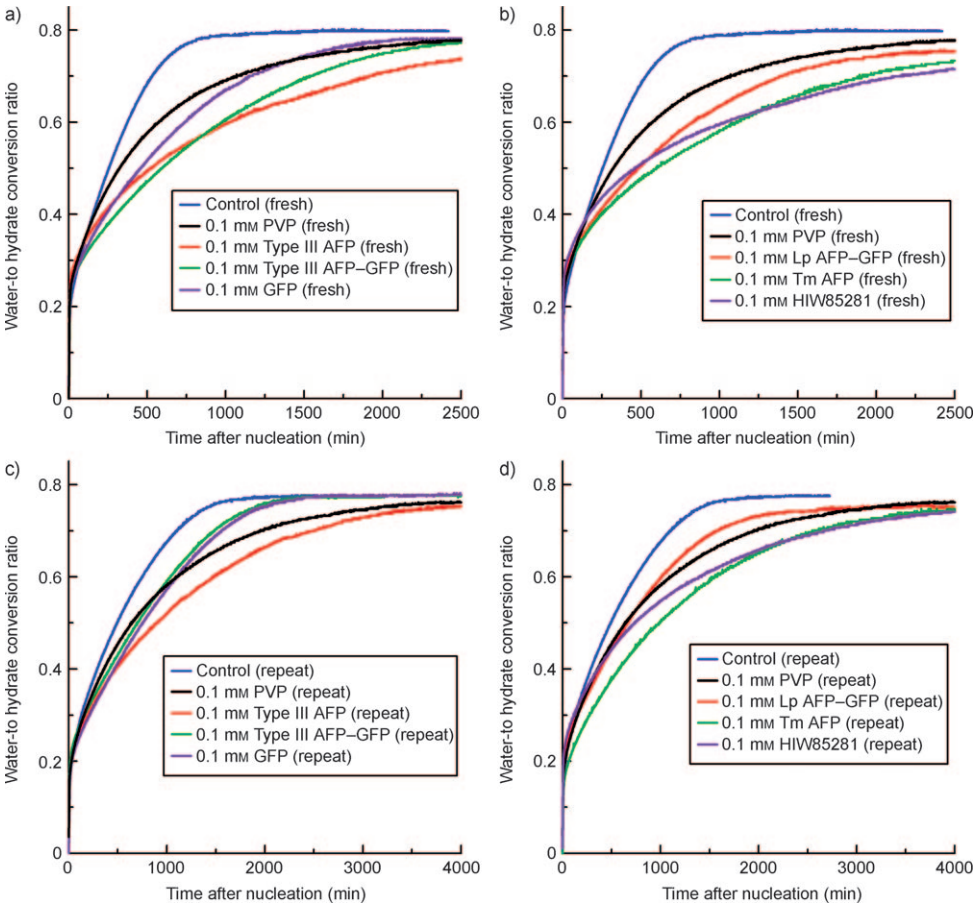

Figure 1. Water-to-hydrate conversion ratio versus time for fresh samples (a and b) and for those obtained after melting and subsequent recrystallization (c and d). The conversion ratios were estimated from the hydrate gas consumptions by assuming sII hydrate with an average cage occupancy of 0.95 (predicted by CSMGem[21]). GFP: green fluorescent protein.

Differential scanning calorimetry (DSC) temperature ramping: In these experiments, the driving force for nucleation, ΔG, increases with a decrease in temperature. DSC was used to monitor hydrate formation, with the observed exothermic peaks corresponding to major hydrate and minor ice nucleation events (Figure 2). The number of exothermic peaks (Figure 2, inset) exceeded the sample cell number (12), which indicated that more than one nucleation event occurred within a single silica gel bead in the capillary. However, upon heating, three peaks were consistently observed: an endothermic event that represented melting ice (−1.5 °C) within the silica gel matrix, along with the other two peaks (5 and 14 °C) that were characteristic of hydrate dissociation and melting. The main hydrate peak is predicted by CSMGem[21] to represent an sII hydrate, whereas the smaller peak most likely indicates a metastable structure I (sI) because its presence in the system was confirmed by in situ X-ray diffraction (not shown). The peak width of the sII hydrate dissociation curve was relatively broad compared with that of the ice peak (Figure 2) and also those of sI (methane) hydrates. Indeed, the peak widths at half height seen here were approximately three times wider than the melting peaks of pure methane hydrates seen in parallel experiments (not shown). This suggests that this single hydrate structure may be somewhat non-uniform. In contrast, pure

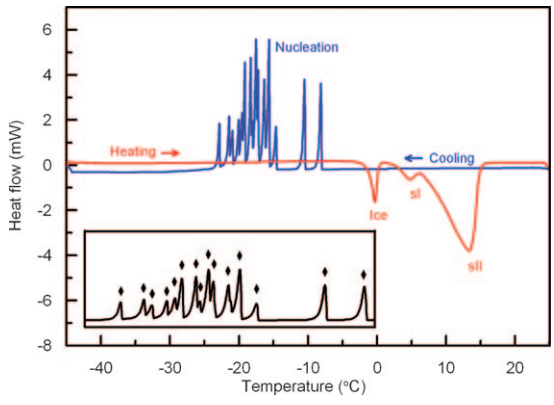

Figure 2. DSC curves with temperature ramping between −45 to 25 °C for the control samples, without additives. Samples (12) were measured at the same time. Each sample was dispersed in silica gel and placed inside an individual capillary tube. The inset magnifies the observed nucleation events, with the diamond symbols representing exothermic peak positions.

phases tend to have sharp melting points, so a homogeneous sII hydrate phase containing the three hydrocarbon guests should still have a sharp melting point and it can be treated as a continuous range of solid solutions as the composition changes within the sII stability region.[23] However, dissociation was initiated at approximately 7 °C, which is about 6 °C lower than the value of 12.7 °C calculated with CSMGem[21] (Figure 2; Table 2). We suggest that the hydrates formed were not equilibrium phases, with both an sI methane hydrate and sII hydrates containing the three hydrocarbons being present, the latter with a range of compositions. These observations agree with previous reports of the nucleation of multiple structures in the same experiment.[24,25]

Table 2. Heats of fusion (melting and freezing) and melting points observed during the DSC temperature ramping experiment with fresh samples and previously crystallized samples containing different inhibitors.

Fresh samples	$H_{m,ice}$ [J][a]	$H_{m,sI}$ [J][a]	$H_{m,sII}$ [J][a]	$H_{m,total}$ [J][a]	$H_{f,total}$ [J][b]	$T_{m,sI}$ [°C][c]	$T_{m,sII}$ [°C][c]
control	1.2	1.5	13.2	16.0	11.9	2.9	7.2
type III AFP	0.6	1.3	15.2	17.0	12.5	2.9	6.9
type III AFP–GFP	0.5	1.4	14.2	16.1	11.6	2.8	7.2
LpAFP–GFP	1.3	1.6	13.4	16.3	12.0	3.2	6.7
TmAFP	0.5	1.4	14.9	16.8	12.4	3.0	7.0
GFP	1.0	1.1	13.7	15.8	11.6	2.9	7.0
PVP	1.2	1.4	13.3	15.9	11.8	3.1	7.1
HIW85281	0.9	1.4	14.5	16.8	12.4	3.2	6.8
Recrystallized samples	$H_{m,ice}$ [J][a]	$H_{m,sI}$ [J][a]	$H_{m,sII}$ [J][a]	$H_{m,total}$ [J][a]	$H_{f,total}$ [J][b]	$T_{m,sI}$ [°C][c]	$T_{m,sII}$ [°C][c]
control	0.4	1.1	14.9	16.4	12.5	3.2	7.9
type III AFP	0.2	0.8	16.2	17.2	13.1	2.8	7.6
type III AFP–GFP	0.2	0.8	15.1	16.1	12.2	2.7	7.6
LpAFP–GFP	0.7	1.0	14.9	16.7	12.4	3.1	7.5
TmAFP	0.3	0.9	15.8	17.0	12.9	2.8	7.7
GFP	0.4	0.7	14.9	16.0	12.2	2.7	7.8
PVP	0.4	0.9	15.0	16.4	12.5	3.2	7.8
HIW85281	0.4	0.9	15.8	17.1	12.8	3.1	7.5

[a] H_m: heat of melting; estimated from the peak area of the endothermic event for ice, sI hydrate, sII hydrate, and all peaks (total). [b] H_f: heat of freezing; calculated by integrating all exothermic peaks. [c] T_m: melting point; measured as the onset of the melting peak for the sI and sII hydrates.

To further investigate the nucleation processes, the observed exothermic peaks were integrated as a function of time during temperature ramping (Figure 3). The sharp profiles of the exothermic peaks (for example, Figure 2) indicated that crystal nucleation was followed by rapid growth due to the large surface area of the sample, small sample volume, and high driving force for hydrate formation. Therefore, the peak positions reflect nucleation events, with the integrated area of the exothermic peaks representing a measure of the conversion into the solid. The samples containing AFPs (type III AFP, type III AFP–GFP, LpAFP, TmAFP) and HIW85281 had somewhat higher cumulative heat values, which were achieved a little later than those of the control samples or PVP (Figure 3; Table 2a). This suggests that there was slightly less metastable sI hydrate formed because sII crystals show more released heat. This interpretation was substantiated when the crystallized samples were subsequently melted and refrozen. Although the profiles of the cumulative heat of reaction were similar for the fresh and recrystallized samples, most of the latter (except type III AFP–GFP) had slightly higher ($\approx$4%) total heats of reaction than the fresh samples. Again, this is most likely because more sII hydrate was formed when the same samples were recrystallized (Table 2b). It should also be noted that the observed difference in the cumulative heats of reaction for DSC runs on the various inhibited samples decreased as the driving force increased, with these values reaching a plateau at around −22 °C.

Endothermic peak analyses, on the other hand, showed little difference in the latent heats for sI and sII hydrates, and there was no clear correlation with the inhibition performance of the different additives (Table 2). Indeed, an estimate of the total heat of reaction from the exothermic peaks was only two-thirds of that calculated from the endothermic peaks, which suggests that, after rapid nucleation, slower transitions such as ice to hydrate or sI hydrates to sII crystals and changes in the guest gas compositions will take place until equilibrium is reached. Such gradual processes resulted in little or no obvious changes in the DSC profiles. The ice endothermic peak, however, did differ between samples in that, in the presence of AFP, the capillary tubes contained less ice than the control samples (except LpAFP–GFP).

DSC isothermal analysis: When the samples were subjected to an isothermal regime (constant driving force, ΔG), sharp exothermic peaks in the DSC profile again indicated nucleation events (Figure 4). When the samples were subsequently heated, two peaks representing melting sI and sII hydrate were observed at temperatures similar to those observed in the temperature-ramping experiments (Figure 4, Table 3). No DSC peak representing ice melting was seen for any of the samples (Figure 4).

The exothermic peaks were integrated to analyze the hydrate nucleation processes (Figure 5), with the recrystallization experiments giving similar results. There was no difference in the cumulative latent heats at the end of the reaction in fresh and recrystallized samples, with the exception of slightly smaller amounts of sI and more sII hydrate (not shown). When the cumulative heats of reaction were compared, all of the AFP-containing samples showed considerably delayed nucleation, whereas samples containing GFP, PVP, and HIW85281 nucleated faster (Figure 5). For the GFP, PVP, and HIW85281 samples, the total heat of melting was about the same as that observed in the temperature-ramping experiments, in which all samples were forced to crystallize quickly (Table 2 and Table 3). This suggests that almost all of the samples with these additives nucleated during the isothermal regimen. In contrast, the relatively smaller heats of melting in the presence of AFPs indicated

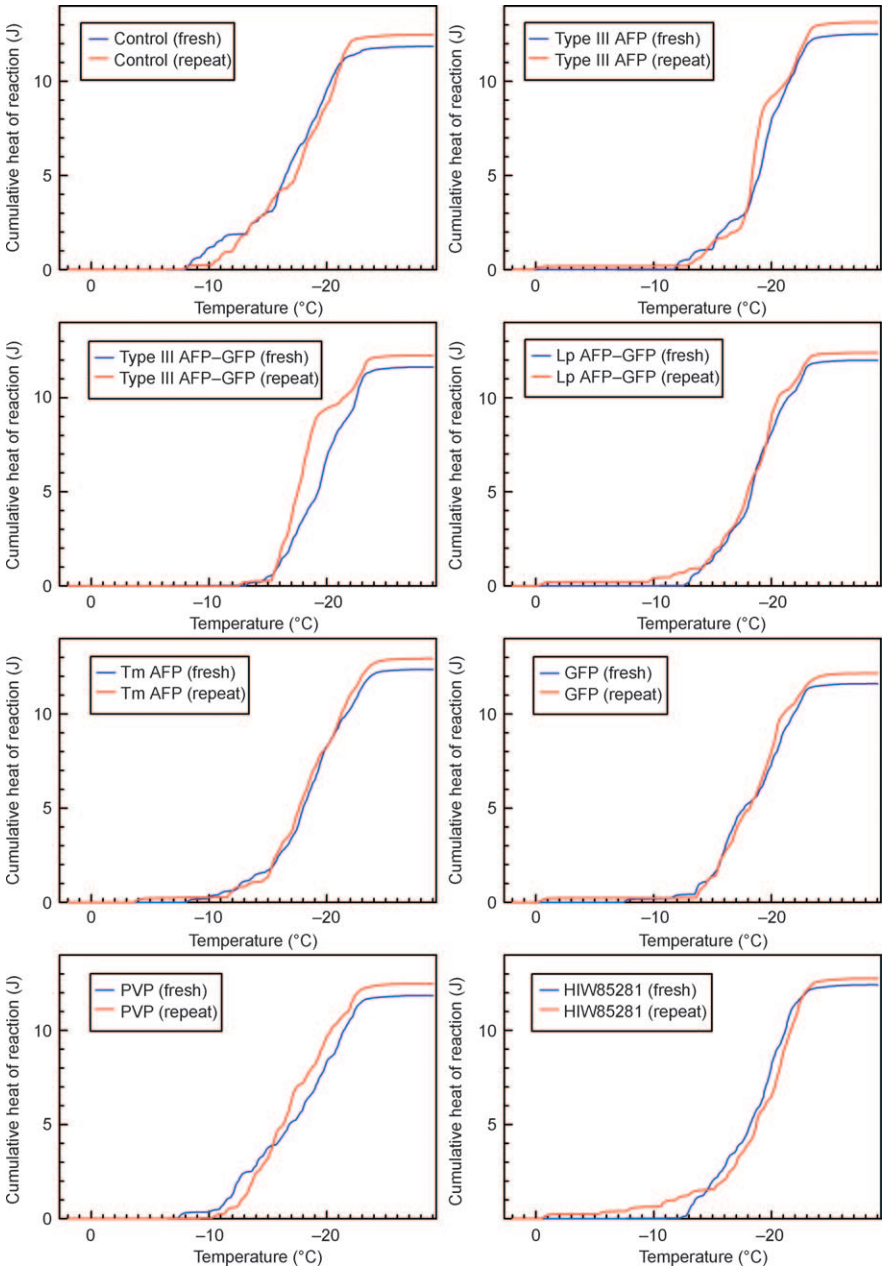

Figure 3. Integration of the exothermic peaks observed during the DSC temperature-ramping experiments versus temperature. Each curve represents the integrated average of 36 samples.

that portions of the samples in the capillary tubes remained unfrozen at the conclusion of the experiments. Of the AFPs tested, type III AFP showed the lowest cumulative heat and was superior to type III AFP–GFP, as in the case of the gas uptake measurements (Figure 5a and c; Table 3). Significantly, the AFP-mediated delay of nucleation persisted through a freeze-and-thaw cycle because the cumulative heat of reaction was similar when the isothermal experiments were repeated with the thawed samples (Figure 5).

Relationship between nucleation and growth inhibitions: In principle, materials to control the formation of gas hydrate plugs may operate either to inhibit nucleation of the hydrate, its growth, or both. In fact, both of these functions have been attributed to various KHIs[6] but without much of an attempt to isolate these rather different modes of action. In our experiments, it is clear that performance as a nucleation inhibitor could not be correlated with growth inhibition. For example, HIW85281 did not show significant inhibition of nucleation in the DSC isothermal experiments (Figure 5), but it was one of the best growth inhibitors (Figure 1); type III AFP was superior to TmAFP in terms of nucleation inhibition (Figure 5), but both of these AFPs showed similar growth inhibition activity (Figure 1). The difference in the two modes of action suggests that KHIs can adsorb to at least two different substrates. To inhibit the heterogeneous nucleation of hydrates, KHIs need to interact with prenucleation clusters and/or foreign materials that act as nucleation templates, thus "poisoning" the nucleation sites. On the other hand, postnucleation growth inhibition requires the adsorption of KHIs on hydrate crystal surfaces. Thus, the prenucleation hydrate clusters and/or associated foreign material with nucleation sites and the hydrate crystals must present different surface structures for inhibitor adsorption. It can be reasoned, however, that good nucleation sites for hydrate crystallization, perhaps with some templating function and complementarity to some hydrate crystal planes, will be good sites for inhibitor adsorption as well. Other nucleation and growth inhibition mechanisms have been suggested. Some molecular dynamics simulations[26] have indicated that KHIs can perturb the structure of liquid water and thus suppress hydrate nucleation and that they therefore do not require surface adsorption. However, this would imply a homogeneous nucleation mechanism. Although there have not been exhaustive studies in this area, it is already known that AFPs do not affect the homogeneous nucleation tempera-

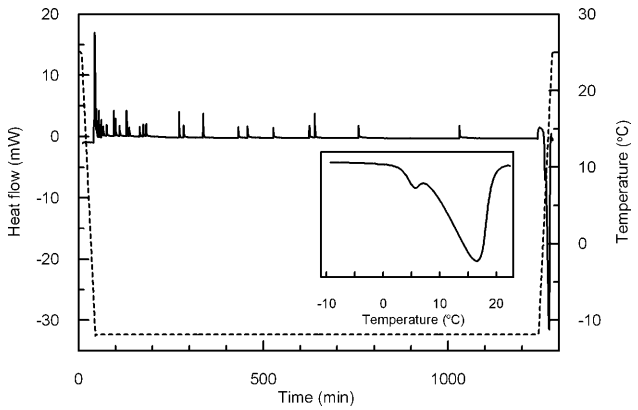

Figure 4. A representative DSC curve (solid line) for the isothermal temperature experiments (−12 °C; broken line) for the control samples. Each sample (12) was confined in silica gel and placed inside an individual capillary tube. The inset magnifies the DSC profile during heating.

Table 3. Heats of fusion and melting points recorded during the DSC isothermal experiments for the various tested inhibitors.

	$H_{m,ice}$ [J]	$H_{m,sI}$ [J][a]	$H_{m,sII}$ [J][a]	$H_{m,total}$ [J][a]	$H_{f,total}$ [J][b]	$T_{m,sI}$ [°C][b]	$T_{m,sII}$ [°C][c]
control	–	1.7	14.2	15.9	15.3	2.7	6.7
type III AFP	–	1.0	10.8	11.8	10.0	2.9	6.9
type III AFP–GFP	–	2.0	12.7	14.7	12.9	3.1	6.6
LpAFP–GFP	–	1.3	12.0	13.3	11.9	2.7	6.9
TmAFP	–	1.3	11.7	13.0	12.1	2.8	6.7
GFP	–	2.0	14.4	16.4	15.5	2.9	6.6
PVP	–	1.8	14.5	16.3	15.1	3.0	7.0
HIW85281	–	2.0	14.1	16.1	15.1	3.1	6.7

[a] The H_m values were estimated from the peak areas of the endothermic events for ice, sI hydrate, sII hydrate, and all peaks. [b] The H_f values were calculated by integrating all exothermic peaks. [c] The T_m values were measured as the onset of the melting peaks for the sI and sII hydrates.

ture of THF hydrate significantly,[15] which suggests that AFPs do not perturb the structure of liquid water.

Time dependence of nucleation inhibition: Our results have also shown that nucleation inhibition with KHIs is a function of time. For example, type III AFP–GFP demonstrated the greatest subcooling for nucleation during relatively fast DSC temperature ramping (Figure 3), but it was considerably worse than type III AFP in the longer DSC isothermal runs (Figure 5). Also, the nucleation temperature of HIW85281 was comparable with those of type III AFP and LpAFP–GFP (Figure 3); however, the profile of the cumulative heat of reaction for the commercial inhibitor was similar to that observed without inhibitors during isothermal runs (Figure 5). These seemingly paradoxical observations can be reconciled with the understanding that hydrate nucleation in an inhibited system is stochastic and can change over time, even under constant temperature and pressure conditions. Indeed, in the first few hours of the DSC isothermal observations, type III AFP–GFP showed the best performance, which mirrored its highest subcooling properties in the temperature-ramping experiments. Within the same time frame, HIW85281 had inhibition effects similar to those of the AFPs (Figure 5) and a similar performance to that in the ramping experiments (Figure 3). These observations are also consistent with the gas-uptake measurements, because for short induction times (up to a few hours), all of the additives worked well as nucleation inhibitors (Table 1). This finding has significant implications in the testing of nucleation inhibition with KHIs because the fluid residence time in a pipeline can reach several days[7] and may become even longer for deep-sea fields. Therefore, long-term measurements are essential to evaluate the ability of additives as nucleation inhibitors.

It should be noted that all of the AFPs studied showed considerably slower nucleation rates than the control and synthetic-inhibitor additives for the 20 h DSC measurements (Figure 5). These results suggest that AFPs have a remarkable ability to maintain their nucleation inhibition effects over long periods and, therefore, should be further explored for their potential as 'longer period' hydrate inhibitors.

Effectiveness of inhibitors after a freeze–thaw cycle: Significantly, AFP-mediated delay of hydrate formation persisted through a freeze-and-thaw cycle. When the gas-uptake experiments were repeated, type III AFP and TmAFP showed the best growth inhibition and matched that of HIW85281 (Figure 1). On the other hand, type III AFP–GFP and LpAFP–GFP showed intermediate values and appeared inferior to the benchmark commercial inhibitor, PVP, unlike the results obtained before crystallization (Figure 1). Although the induction times became shorter than those in the first crystallization experiments due to the memory effect, the gas-uptake observations also indicated delays of hydrate induction periods in the presence of AFPs. In the DSC temperature-ramping and isothermal experiments, freeze–thaw cycles did not significantly affect the observations showing strong hydrate nucleation inhibition by AFPs during recrystallization, which were comparable to the results from the initial runs (Figure 3 and Figure 5). Again, the observed robustness of AFPs is important for practical applications because the melting and reformation of gas hydrates could take place in actual pipelines.

Relationship between hydrate and ice inhibition: Ice and sII hydrate structures are clearly distinct, with ice presenting a hexagonal structure with O atoms at different distances depending upon the crystal plane and the cubic sII hydrate having an octahedral morphology. Nevertheless, AFPs do appear to adsorb and become incorporated into both ice and hydrate crystals.[13] Herein, our experiments go further and clearly show that the efficacy of a particular AFP towards hydrate is not correlated with its TH towards ice. TH activity derives from adsorption onto bulk ice after nucleation, so it is reasonable to compare the TH activities with observed postnucleation hydrate growth inhibition. Al-

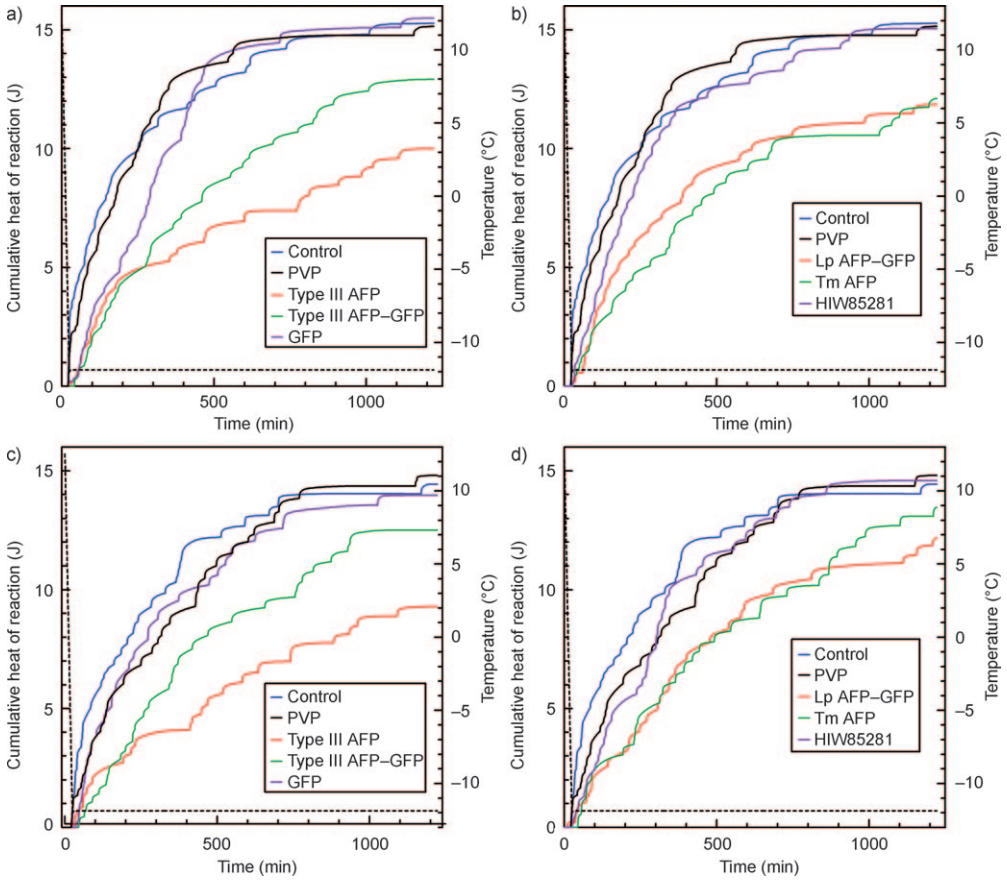

Figure 5. The cumulative heat of reaction for fresh samples (a and b) and for the same samples after melting and subsequent recrystallization (c and d) as estimated by integrating exothermic peaks observed during the DSC isothermal run at −12 °C. Each result is statistically based on 36 samples.

though the TH value of TmAFP is approximately an order of magnitude larger than that of type III AFP, these proteins showed similar inhibition activities on hydrate growth (Figure 1). Type III AFP and type III AFP–GFP have comparable TH values, but type III AFP–GFP was significantly inferior to type III AFP in terms of hydrate growth inhibition and behaved similarly to LpAFP–GFP, which has a very low TH value. The reverse is also true, because the hydrate inhibitor PVP has no TH activity toward ice, and a mutant type I AFP with no measurable TH value still showed hydrate inhibition.[15,27] Perhaps these observations should not be surprising because it is known that some AFPs have surface complementarity to only specific crystallographic planes of ice.[8] Nevertheless, experiments to investigate the residues that are important for hydrate adsorption are now underway.

AFPs might be able to prevent ice from nucleating, because it has been suggested that they adsorb to ice surfaces by first forming clathrate structures that then become incorporated into bulk ice.[28,29] However, the relative activities of AFPs on ice nucleation are unknown, so we cannot compare them with hydrate nucleation. Differences in the amount of ice formed with the various inhibitors in the DSC temperature-ramping experiments (Table 2) do not reflect ice inhibition because the observed endothermic peaks do not represent the original ice content. As previously mentioned, the differences between the exothermic peak areas and those corresponding to the exothermic bands indicate that there was considerable transformation from ice to hydrate after nucleation and the interconversion rate was probably dependent on the presence of additives. Further studies are required to address this issue.

Conclusion

This study demonstrates that the application of high-pressure DSC with samples dispersed in silica gel provides a powerful method for screening candidate KHIs and can generate sufficient data for statistical analysis. All of the additives tested, including four AFPs and two synthetic KHIs, showed significant nucleation inhibition for the short-term observations of gas uptake and the DSC temperature-ramping experiments, whereas only the AFPs appeared to prolong the induction periods considerably. These observations clearly suggest that nucleation inhibition by KHIs is a time-dependent process and the AFPs have a superior ability to prevent nucleation under these conditions. Gas-uptake results also show that the AFPs are more effective than a basic commercial inhibitor (PVP) but not all AFPs are sig-

nificantly different from HIW35281, a new and very effective KHI. There was no clear correlation between the effectiveness of the nucleation and growth inhibitions, which indicates a distinct difference in the adsorption sites or inhibition. AFP activity towards hydrates is not necessarily reflected in their activity toward ice, a result implying the inhibition mechanisms must differ in detail. Nevertheless, the robustness of AFPs during freeze–thaw cycles and during long-term experiments argues for their potential value as new KHIs. Taken together, these findings have significant implications for the development of high-performance 'green' hydrate inhibitors for pipeline flow assurance. The methodology developed will also allow the efficient characterization of potential inhibitors and thus give data essential for developing an understanding of how such inhibitors interact with hydrates during the various and complex phases of hydrate formation.

Experimental Section

Materials: AFPs were produced recombinantly in *Escherichia coli* BL21 cells by either using shake flasks or a bioreactor, as previously described.[13] The presence of a poly-$(His)_6$ sequence tag on all of the proteins facilitated their purification with metal-affinity chromatography.[13] Some AFPs were previously shown to be more stable under hydrate-forming conditions when expressed as fusion proteins,[13] so a GFP (25 kDa) sequence was also ligated to certain AFP coding regions. The tested proteins included a low-ice-activity LpAFP–GFP with a mean TH value of 0.10 °C (41 kDa), a moderately active ocean pout type III AFP (TH = 0.43 °C, 6.8 kDa), and a type III AFP–GFP (TH = 0.48 °C, 32 kDa), as well as a 'hyperactive' TmAFP (TH = 3.5 °C, 8.4 kDa). GFP (TH = 0 °C), purified as for use with the AFPs, was used as a non-AFP control protein. The TH values were determined on purified proteins at approximately 4 mg mL^{-1}. Before the experiments, all buffer salts used for protein production and purification were removed by dialysis against deionized water. For comparison with AFPs, PVP (PVP10; Sigma Aldrich, 10 kDa) and HIW85281 (a proprietary commercial product of unknown composition, 3 kDa) were used. All chemicals, including the recombinant proteins, were diluted to 0.1 mM solutions in deionized water.

Due to the limited amount of recombinant AFPs, a method to overcome this restriction and to ensure efficient hydrate nucleation was devised. Solutions were dispersed in silica gel beads with a size range of 70–200 μm, a 1000 Å average pore diameter, and a 0.83 mL g^{-1} pore volume (Silicycle). The use of silica gel increases the area of the water–gas interfaces and thus facilitates gas hydrate nucleation and growth;[30] the pore size is large enough so that the thermodynamics of hydrate formation will not deviate markedly from those of a bulk system. Silica gel is amorphous, so it presents a disordered hydrophilic surface to the hydrate-forming solutions on initial hydrate formation; thus, there is a constant background of interactions for all samples. In an effort to use guest gases that mimic natural gas, a gas mixture of methane–ethane–propane (93% C_1, 5% C_2, and 2% C_3; Praxair) was employed.

Gas uptake: The hydrate induction time and growth rate were assessed by pressure changes. Deionized water (1 mL) or the appropriate test solution and silica gel (1.3 g) were placed in a glass beaker and mixed with a stainless-steel spatula. The wet silica gel was then loaded into a stainless-steel high-pressure cell with an inner volume of approximately 30 cm^3, and the cell was immersed into a 25 °C water bath. The system was pressurized with the $CH_4/C_2H_6/C_3H_8$ gas mixture to 7 MPa. The sample pressure was monitored with a transducer connected to the cell and a data logger (Omega, OM-DAQPRO-5300). After the system reached equilibrium, the cell was transferred within a few seconds to a 0.5 °C water bath, and hydrate nucleation was observed as a sudden pressure drop. Measurements were repeated with the same samples to test the effect of a freeze–thaw cycle on AFP activity (after dissociation for 2 h at 25 °C). All samples were tested twice with the exception of TmAFP, which was tested once due to the paucity of material. In all samples, the hydrate growth was reproducible with superimposable plots of gas consumption over time for each repeated sample run (not shown).

DSC temperature ramping: A high-pressure microdifferential scanning calorimeter (DSC; Setaram Inc, μ-DSC VII) was employed to observe the gas hydrate nucleation temperatures. Silica gel (≈1.8 mg) was placed in a borosilicate capillary tube (1 cm × 1 mm inner diameter) that had been heat sealed at one end. Pure water (1 μL) or the same volume of the appropriate test solution was injected into the tube with a microsyringe (Hamilton). Capillaries with the same samples (12) were loaded into a high-pressure DSC cell together (samples were separated in capillaries, so a nucleation event in one sample will not affect others). Subsequently, the system was pressurized with the $CH_4/C_2H_6/C_3H_8$ gas mixture to 4 MPa, with the pressure remaining constant during the experiments. For temperature ramping, the system was cooled from 25 to −45 °C (at 0.25 °C min^{-1}) and then heated to 25 °C at the same rate. In total, 36 samples (12 × 3) were tested for each different inhibitor and the controls. The effect of a freeze–melting cycle was observed by repeating the measurement with the same samples; the interval between the first and second runs was 10 min at 25 °C.

DSC isothermal determinations: Hydrate nucleation was also investigated by using isothermal experiments monitored by DSC. Sample preparation was essentially the same as that described for the DSC temperature ramping, and the 4 MPa methane–ethane–propane gas mixture was used for all experiments. After sample loading in the DSC cell, the temperature was reduced from 25 to −12 °C at 1 °C min^{-1} and kept constant for 20 h. After that time, the samples were again heated to 25 °C (at 1 °C min^{-1}). The total number of samples measured for each test solution was 36, and the experiment was repeated twice for the same samples with a 10 min interval, in order to study the effect of a freeze–thaw cycle.

Analysis: To investigate the hydrate nucleation events, the observed DSC exothermic peaks were integrated as a function of time. When measurements were repeated with fresh control samples, the profiles of the integrations were reproducible with calculated average differences in the cumulative heat of reaction of 0.5 J for both the temperature-ramping and isothermal experiments (not shown). However, as latent heats depend on temperature, the cumulative heats of reaction were not expected to be identical in different experiments. The statistical thermodynamics program CSMGem[22] was used for statistical analysis.

Acknowledgements

We are grateful for the support of this research by the Natural Sciences and Engineering Research Council of Canada and Shell Global Solutions. The authors also thank Dr. Rajnish Kumar for fruitful discussion.

[1] a) "Hydrate inclusion compounds": G. A. Jeffrey in *Comprehensive Supramolecular Chemistry, Vol. 6: Solid-state Supramolecular Chemistry: Crystal Engineering* (Eds.: J. L. Atwood, J. E. D. Davies, D. D. MacNicol, F. Vogtle), Pergamon, Oxford, **1996**; b) "Stoichiometry and Thermodynamics of Clathrate Systems": Yu. A. Dyadin, V. R. Belosludov in *Comprehensive Supramolecular Chemistry, Vol. 6: Solid-state Supramolecular Chemistry: Crystal Engineering* (Eds.: J. L. Atwood, J. E. D. Davies, D. D. MacNicol, F. Vogtle), Pergamon, Oxford, **1996**; c) "Clathrate Hydrates": D. W. Davidson in *Water: A Comprehensive Treatise, Vol. 3* (Ed.: F. Franks), Plenum, New York, **1972**; d) "Clathrate Hydrates": J. A. Ripmeester, C. I. Ratcliffe, K. A. Udachin in *Supramolecular Chemistry* (Eds.: J. A. Atwood, J. Steed), Marcel Dekker, New York, **2004**, pp. 274–280.
[2] G. J. MacDonald, *Ann. Rev. Energy* **1990**, *15*, 53–83.
[3] A. V. Milkov, G. E. Claypool, Y.-J. Lee, W. Xu, G. R. Dickens, W. S. Borowski, *Geology* **2003**, *31*, 833–836.

[4] a) E. D. Sloan, *Energy Fuels* **1998**, *12*, 191–196; b) C. A. Koh, E. D. Sloan, *AIChE J.* **2007**, *53*, 1636–1643.
[5] E. D. Sloan, C. A. Koh, *Clathrate Hydrates of Natural Gases*, CRC Press, Boca Raton, **2007**.
[6] M. A. Kelland, *Energy Fuels* **2006**, *20*, 825–847.
[7] J. P. Lederhos, J. P. Long, A. Sum, R. L. Christiansen, E. D. Sloan, *Chem. Eng. Sci.* **1996**, *51*, 1221–1229.
[8] Y. Yeh, R. E. Feeney, *Chem. Rev.* **1996**, *96*, 601–618.
[9] Z. Jia, P. L. Davies, *Trends Biochem. Sci.* **2002**, *27*, 101–106.
[10] a) C. Sidebottom, S. Buckley, P. Pudney, S. Twigg, C. Jarman, C. Holt, J. Telford, A. McArthur, D. Worrall, R. Hubbard, P. Lillford, *Nature* **2000**, *406*, 256; b) M. J. Kuiper, P. L. Davies, V. K. Walker, *Biophys. J.* **2001**, *81*, 3560–3565.
[11] G. L. Fletcher, C. L. Hew, P. L. Davies, *Annu. Rev. Physiol.* **2001**, *63*, 359–390.
[12] L. A. Graham, Y.-C. Liou, V. K. Walker, P. L. Davies, *Nature* **1997**, *388*, 727–728.
[13] R. Gordienko, H. Ohno, V. K. Singh, Z. Jia, J. A. Ripmeester, V. K. Walker, *PLoS ONE* **2010**, *5*, e8953.
[14] H. Zeng, L. D. Wilson, V. K. Walker, J. A. Ripmeester, *Can. J. Phys.* **2003**, *81*, 17–24.
[15] H. Zeng, L. D. Wilson, V. K. Walker, J. A. Ripmeester, *J. Am. Chem. Soc.* **2006**, *128*, 2844–2850.
[16] a) S. Alavi, R. Susilo, J. A. Ripmeester, *J. Chem. Phys.* **2009**, *130*, 174501; b) S. Alavi, K. A. Udachin, J. A. Ripmeester, *Chem. Eur. J.* **2010**, *16*, 1017–1025.
[17] H. Zeng, I. L. Moudrakovski, J. A. Ripmeester, V. K. Walker, *AIChE J.* **2006**, *52*, 3304–3309.
[18] T. Uchida, I. Y. Ikeda, R. Ohmura, S. Tsuda in *Physics and Chemistry of Ice* (Ed.: W. F. Kuhs), RSC, Cambridge, **2007**, pp. 609–618.
[19] S. Al-Adel, J. A. G. Dick, R. El-Ghafari, P. Servio, *Fluid Phase Equilib.* **2008**, *267*, 92–98.
[20] "The search for green inhibitors: Perturbing hydrate growth with bugs": E. I. Huva, R. V. Gordienko, J. A. Ripmeester, H. Zeng, V. K. Walker, Proceedings of 6th International Conference on Gas Hydrates, **2008**.
[21] A. L. Ballard, E. D. Sloan, *Fluid Phase Equilib.* **2002**, *371*, 194–197.
[22] J. D. Lee, P. Englezos, *Chem. Eng. Sci.* **2005**, *60*, 5323–5330.
[23] J. H. Van der Waals, J. C. Platteeuw, *Adv. Chem. Phys.* **1958**, *2*, 1.
[24] a) D. K. Staykova, W. F. Kuhs, A. N. Salamantin, T. Hansen, *J. Phys. Chem. B* **2003**, *107*, 10299–10311; b) J. M. Schicks, J. A. Ripmeester, *Angew. Chem.* **2004**, *116*, 3372–3375; *Angew. Chem. Int. Ed.* **2004**, *43*, 3310–3313.
[25] J. Zhang, R. W. Hawtin, Y. Yang, E. Nakagava, M. Rivero, S. K. Choi, P. M. Rodger, *J. Phys. Chem. B* **2008**, *112*, 10608–10618.
[26] a) R. W. Hawtin, C. Moon, P. M. Rodger, *Proceedings of 5th International Conference on Gas Hydrates* **2005**, *1*, 317–321; b) C. Moon, R. W. Hawtin, P. M. Rodger, *Faraday Discuss.* **2007**, *136*, 367–382; c) R. W. Hawtin, D. Quigley, P. M. Rodger, *Phys. Chem. Chem. Phys.* **2008**, *10*, 4853–4864.
[27] "The mysteries of memory effect and its elimination with antifreeze proteins": V. K. Walker, H. Zeng, R. V. Gordienko, M. J. Kuiper, E. I. Huva, J. A. Ripmeester, Proceedings of 6th International Conference on Gas Hydrates, **2008**.
[28] A. Cheng, K. M. Merz, *Biophys. J.* **1977**, *17–20*, 2851–2873.
[29] C. Yang, K. A. Sharp, *Proteins Struct. Funct. Bioinf.* **2005**, *59*, 266–274.
[30] Y. Seo, I. L. Moudrakovski, J. A. Ripmeester, J. Lee, H. Lee, *Environ. Sci. Technol.* **2005**, *39*, 2315–2319.

Received: November 21, 2009
Revised: April 11, 2010
Published online: July 12, 2010

